

# Parallel vortex shedding at $Re = O(10^4)$ – a transverse control cylinder technique approach

By S. C. LUO AND H. M. XIA

Department of Mechanical Engineering, National University of Singapore,  
10 Kent Ridge Crescent, Singapore 119260

(Received 1 July 2004 and in revised form 5 April 2005)

In the present studies, the effects of the end conditions of a circular cylinder on its wake at a fairly high Reynolds number of  $Re = 1.57 \times 10^4$  were studied. The transverse control cylinder technique (TCCT) was previously reported to be able to induce parallel vortex shedding at  $Re = O(10^2)$ . In the present work, experimental results showed that the TCCT is still effective in inducing parallel vortex shedding at  $Re = O(10^4)$ . Initially, before the inclusion of the control cylinders, vortices shed by the main cylinder were curved (all shapes referred to are time-averaged shapes) owing to the influence of the cylinder end conditions. Later, two larger control cylinders of diameter  $D$  were included and were located normal and upstream of the main cylinder near its ends to change its end conditions. By manipulating the control distance (the gap between the control cylinders and the main cylinder), different vortex-shedding patterns could be induced. With both control cylinders fixed at the optimum control distance of  $L_1 = L_2 = L_0 = 1.26D$ , the main cylinder was induced to shed parallel vortices. For the cases of curved vortex shedding (without control cylinders) and parallel vortex shedding (with control cylinders at the optimum distance of  $L_1 = L_2 = L_0 = 1.26D$ ), various aerodynamic parameters of the main cylinder were measured and compared. Results showed that the inclusion of the control cylinders speeded up the flow velocity at the ends of the main cylinder and led to a more uniform pressure distribution over the central span of the main cylinder, which finally resulted in parallel vortex shedding. Aerodynamic parameters such as drag coefficient and Strouhal number associated with parallel vortex shedding were found to be larger than their curved shedding counterparts. However, extra caution should be exercised in interpreting their implications as these data were under the influence of additional wind-tunnel blockage caused by the presence of the control cylinders. Preliminary and approximate calculations had shown that blockage effects were likely to be responsible for a significant part in the change in the aerodynamic parameters such as the drag coefficient and Strouhal number when the control cylinders were installed. When the control cylinders were symmetrically placed, but not at the optimum distance ( $L_1 = L_2 \neq L_0$ ), the vortex-shedding pattern became curved, and was concave or convex downstream at  $L_1 = L_2 < L_0$  or  $L_1 = L_2 > L_0$ , respectively. When the control cylinders were asymmetrically placed ( $L_1 \neq L_2$ ), oblique vortex shedding was induced, with the oblique vortex slanting in the same way as the straight line joining the centres of the control cylinders. The relation between the Strouhal numbers for parallel and oblique vortex shedding was found to still follow the cosine law. The present work confirms earlier finding by other workers that a non-uniform spanwise base pressure distribution was the cause of spanwise base flow, which led to curved or oblique vortex shedding.

---

## 1. Introduction

From the literature, it is known that the end conditions of a circular cylinder affect its wake at low Reynolds number ( $Re$ ). Even for a very slender cylinder, parallel vortex shedding only exists at very low Reynolds numbers. When  $Re$  increases to a certain magnitude ( $\approx 72$ , according to Hammache & Gharib 1989), oblique shedding where vortices are shed at a certain angle to the axis of the cylinder occurs. Since the report of the slantwise vortex-shedding phenomenon by Berger (1964), much work has been carried out on the transition from parallel to oblique shedding. Oblique vortex shedding was once interpreted as a secondary instability in the flow, and its onset was considered as Reynolds-number dependent. However, in the investigations that followed, there was no consensus on the onset Reynolds number. A relevant phenomenon in that a discontinuity in the Strouhal number ( $St$ ) –  $Re$  curve occurred at a certain Reynolds number was reported by Tritton (1959). Tritton attributed the discontinuity to a transition in the flow. The investigations that followed showed that there can be many reasons for the discontinuities, including a slight shear of the free stream (Gaster 1971; Maull & Young 1973), differences in free-stream turbulence (Berger & Wille 1972), and flow-induced vibration of the cylinder (Van Atta & Gharib 1987), etc. Williamson (1988) found that in the absence of the above-mentioned effects, discontinuities in the  $St$ – $Re$  curve can be caused by non-parallel vortex shedding; and when parallel shedding was obtained, the discontinuities were absent. Slaouti & Gerrard (1981) reported that even in a flow of good quality and with a smooth and straight cylinder, the vortex shedding can still be influenced by the geometry at the cylinder ends. Other experiments also showed that the wall boundary layer can influence the vortex-shedding patterns. Ramberg (1983) found that endplates can affect the pressure near the cylinder ends and the vortex shedding. The boundary conditions at the spanwise ends of the cylinder dictate the angle of shedding over the whole span, even for a cylinder that is hundreds of diameters in length, and this is referred to as ‘indirect influence’ by Williamson (1989). Williamson (1988) observed that the obliquely shed vortices can form a periodic chevron pattern, and the oblique angle at each half of the cylinder was dictated by the end conditions of that half. It was also found that it was possible to promote parallel shedding by manipulating the end conditions of the cylinder (by slightly increasing the free-stream speed near the cylinder ends). Possible methods include the application of suitably inclined end plates (Williamson 1988), use of coaxial end cylinders of larger diameter (Eisenlohr & Eckelmann 1989), the transverse control cylinder technique (TCCT) (Hammache & Gharib 1989, 1991) and the suction tube technique (Miller & Williamson 1994).

The TCCT was proposed by Hammache & Gharib (1989), and is relatively simple to implement. In this technique, two control cylinders are placed normal and upstream of the main cylinder near its ends, and the region of interest is the part of the main cylinder span that comes in between the two control cylinders. The gap between the control cylinders and the main cylinder is termed  $L$  ( $L_1$  and  $L_2$  if the gap sizes at the two ends of the main cylinder are different) (see figure 1). Hammache & Gharib (1989, 1991) worked at Reynolds numbers of up to about 160 and found that at a certain  $L$ , parallel vortex shedding can be induced and, under such a situation, the discontinuities in the  $St$ – $Re$  curve disappear. They also observed that  $L$  is an important factor that affects the vortex-shedding pattern, and by manipulating  $L$ , oblique and curved vortex shedding can also be induced. They pointed out that a non-uniform pressure distribution, which induced a spanwise flow in the base region of the cylinder, was responsible for the oblique shedding; and an even distribution of the base pressure will lead to parallel vortex shedding.

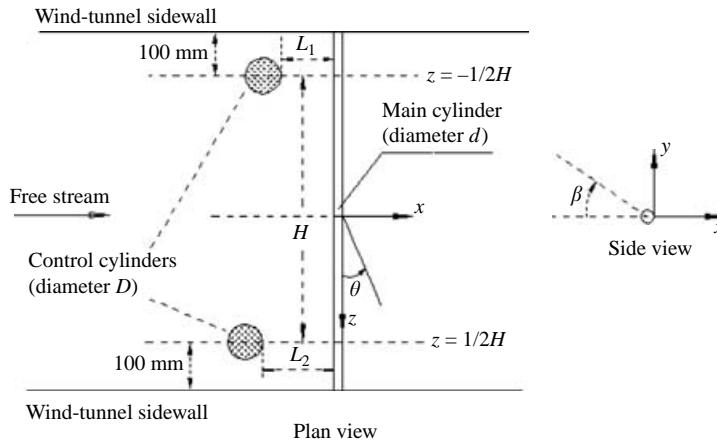


FIGURE 1. Schematics of the experimental set-up and reference coordinate system.

To date, most studies on the effects of end conditions on the cylinder wake were carried out at low Reynolds numbers ( $O(10^2)$ ), and very little work had been done to understand the end effects and the three-dimensional phenomena at mid to high Reynolds numbers. In fact, to the best of our knowledge, the only such investigation was reported by Prasad & Williamson (1997). They studied the effects of end conditions on the cylinder wake at moderately high Reynolds numbers of  $200 < Re < 10000$ . Their study showed that by suitably manipulating the end conditions (they used inclined end plates), it is possible to induce oblique or parallel vortex-shedding patterns across a large part of the cylinder span over a large  $Re$  range. Since the vortex parameters of oblique and parallel vortex shedding are different, if the vortex-shedding patterns can be controlled at high Reynolds number, we can carry out a detailed investigation into these phenomena, and gain further understanding about the wake flow around the cylinder. The present work is an attempt to study the effects of the end conditions of a circular cylinder on its wake flow at a moderately high Reynolds number ( $O(10^4)$ ) by using the TCCT, and to show the feasibility of controlling the vortex-shedding patterns by manipulating the control cylinder positions. A number of measurements were carried out in the present study, they include the vortex-shedding patterns, cylinder surface-pressure distribution, spanwise Strouhal-number distribution, and flow-field velocity, etc. The difference in magnitude of these parameters under different shedding patterns will also be studied.

## 2. Experimental set-up and methods

### 2.1. Experimental set-up

The transverse control cylinders technique was applied during the experiment to modify the end conditions of the circular cylinder. Figure 1 shows part of the experimental set-up, which includes the wind tunnel, a main circular cylinder and two control cylinders that are located upstream and normal to the main cylinder, near its ends.

The wind tunnel used is of the suction design and the fan/motor was located downstream of the test section. It can provide a uniform flow with a turbulent intensity of 0.4%. The test section is 2.8 m in length, 1.0 m in width and 0.6 m in height. A Pitot-static probe was mounted upstream of the main cylinder, and

together with an inclined manometer, it monitored the velocity of the free stream. The experimental uncertainty of the velocity during the measurements was determined to be around 0.6%. A number of slots on the ceiling of the test section allow us to insert hot-wire or Pitot probes for various flow measurements, and all the unused slots were carefully sealed up during the experiments. The main circular cylinder was made of brass with a highly polished surface. Its diameter ( $d$ ) is 25 mm. During the experiment, the main cylinder was mounted horizontally across the test section of the wind tunnel, midway between the ceiling and the floor. It protruded from both sidewalls of the test section and was mounted onto a metal frame. The frame was in turn secured to the ground to minimize the direct transmission of the vibration from the wind tunnel to the main cylinder. The openings of the wind-tunnel sidewalls where the cylinder protruded were also carefully sealed to avoid air leakage. The effective length of the cylinder was therefore 1000 mm (the width of the test section), and its aspect ratio was 40. The main cylinder had 19 (0.6 mm internal diameter) pressure tappings evenly installed along a generator at a distance of 50 mm ( $2d$ ) apart. Based on a test section height of 0.6 m, the blockage ratio of this set-up is 4.17%. The main cylinder was mounted onto the frame in such away that it could be rotated about its axis. An attached circular protractor allowed the azimuth angle ( $\beta$ ) to be accurately determined. During the experiments, once the cylinder was rotated to the desired position, two lock nuts were tightened to prevent accidental rotation.

Two identical larger transverse control cylinders of diameter ( $D$ ) were used to alter the end conditions of the main cylinder. According to Hammache & Gharib (1989), for the control cylinders to be effective,  $D/d$  should be larger than 3. Hammache & Gharib (1989) had a  $D/d$  of 7.8125, whereas Hammache & Gharib (1991) had  $D/d$  with magnitudes of 4.7, 7.875 and 9.75. In the present work, in order to keep the blockage effects at a relatively low level, we used aluminium control cylinders with a diameter of 100 mm. Our  $D/d$  is thus equal to 4. During the experiment, the control cylinders were placed upstream and normal to the main cylinder, and were tightly secured to the ceiling and the floor of the wind tunnel to keep vibrations to a minimum. As shown in figure 1, the control cylinders were positioned such that there was a distance of 100 mm between each cylinder axis and the nearest wind-tunnel vertical sidewall. The crossflow distance between the axes of the control cylinders was designated as  $H$ . The effective aspect ratio of the main cylinder was defined as  $A = H/d$ . In the present set-up,  $A = 32$ . The gap between each control cylinder and the main cylinder was defined as the control distance, and they were denoted as  $L_1$  and  $L_2$  (figure 1). These gap sizes could be varied by moving the control cylinders. As shown in figure 1, the origin of the reference coordinate system was at the base and mid-span of the main cylinder. The positive  $x$ -coordinate was in the streamwise direction and points downstream. The  $y$ -coordinate was set normal to the cylinder axis and was positive upward, while the  $z$ -coordinate was along the span of the main cylinder. Together, the  $x$ ,  $y$ ,  $z$  axes formed a right-hand system. The azimuth angle  $\beta$  was the angle away from the front stagnation point ( $\beta = 0^\circ$  there) of the main cylinder. The vortex-shedding angle  $\theta$  was measured counterclockwise from the positive  $z$ -axis.

## 2.2. Experimental methods

### 2.2.1. Pressure measurement

The surface pressure ( $P$ ) was sensed from pressure taps on the main cylinder surface. The taps were connected through PVC tubes to a 48 channel scanivalve which contained a  $\pm 0.3$  p.s.i. pressure transducer, and could be switched to read

any of the inlet pressure signals. All of the PVC tubes were 1500 mm long. The pressure data were acquired by a data-acquisition card installed in a PC. The flow static pressure was sensed from the sidewall of the wind tunnel, upstream of the main cylinder, with a separate pressure transducer. To calculate the time-averaged pressure coefficient, the pressure signals from both pressure transducers were simultaneously sampled at a frequency of 1000 Hz and over a duration of 10 s.

The pressure coefficient was calculated as

$$C_p = \frac{P - P_s}{\frac{1}{2}\rho U_\infty^2}, \quad (1)$$

where  $P$  = surface pressure of the main cylinder,

$P_s$  = free-stream static pressure,

$\rho$  = density of air,

$U_\infty$  = velocity of the free steam.

From the pressure coefficient calculated by (1), the mean drag and lift coefficients,  $C_D$  and  $C_L$ , respectively, were calculated as

$$C_D = \frac{1}{2} \int_{-\pi}^{\pi} C_p(\beta) \cos \beta \, d\beta, \quad (2a)$$

$$C_L = -\frac{1}{2} \int_{-\pi}^{\pi} C_p(\beta) \sin \beta \, d\beta, \quad (2b)$$

where  $C_p$  = cylinder surface pressure coefficient,

$\beta$  = angular displacement measured from the front stagnation point of the cylinder.

### 2.2.2. Hot-wire anemometry measurement

In the present experiments, hot wires were used to determine the flow velocity at strategic locations, the vortex-shedding frequency and the vortex-shedding patterns. The velocity signal from the hot wire was first sent through a signal filter, and was then sampled by the data acquisition system via an A/D converter.

The vortex-shedding frequency was determined via the usual method of identifying the spectral peak of the wake velocity signal. As in all similar work, the Strouhal number ( $St$ ) is calculated as

$$St = \frac{f_s d}{U_\infty}, \quad (3)$$

where  $St$  = Strouhal number,

$f_s$  = vortex-shedding frequency,

$d$  = diameter of the main cylinder,

$U_\infty$  = velocity of the free stream.

Another application of the hot wire in the present work was in the measurement of the spanwise correlation of the fluctuating velocity signals so that the vortex-shedding pattern can be deduced. The correlation coefficient ( $Cr$ ) between two signals  $U_{1i}$  and  $U_{2i}$  is defined as

$$Cr = \frac{\sum_1^n (U_{1i} - \bar{U}_1)(U_{2i} - \bar{U}_2)}{\sqrt{\sum_1^n (U_{1i} - \bar{U}_1)^2 \sum_1^n (U_{2i} - \bar{U}_2)^2}}, \quad (4)$$

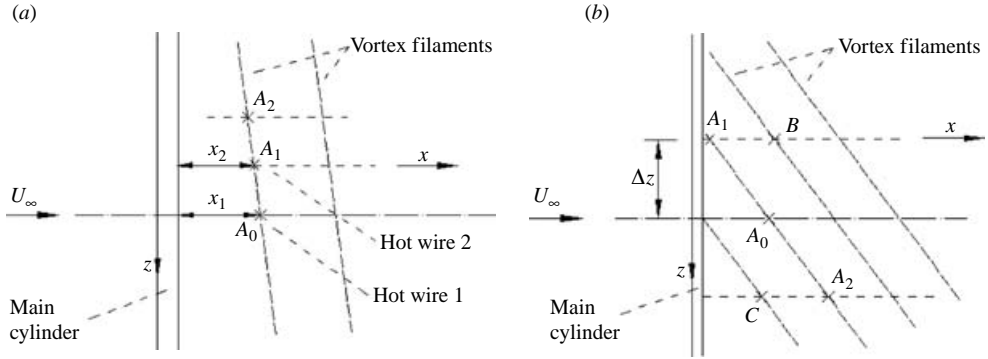


FIGURE 2. (a) Method used to determine the vortex shedding pattern. (b) Schematics of the case under which misleading data of maximum  $Cr$  could be obtained.

where  $U_{1i}$  and  $U_{2i}$  are fluctuating velocity signals from hot wires 1 and 2, respectively, and

$$\bar{U}_1 = \frac{1}{n} \sum_1^n U_{1i}, \quad \bar{U}_2 = \frac{1}{n} \sum_1^n U_{2i},$$

are the time-averaged mean values of the two velocity signals.

The output signals of the two hot wires were sampled simultaneously, and for accuracy the measurement was over more than 800 vortex-shedding cycles. Figure 2(a) illustrates the procedure adopted to determine the vortex-shedding pattern. Hot wire 1 (the reference hot wire) was first positioned at a certain point, say  $A_0(x_1, y_1, z_1)$ , while hot wire 2 was positioned at  $(x_2, y_2, z_2)$ , where  $y_2 = y_1$  and  $|z_2 - z_1| = \Delta z$ . Then, hot wire 2 was moved in the  $x$  direction ( $x_2$  varied) at an increment of  $\Delta x$ . At each point, the correlation coefficient between the two hot-wire signals was computed and recorded. If a maximum in the correlation coefficient was obtained when hot wire 2 was at a position denoted by  $A_1$ , then the vortex shedding at points  $A_0$  and  $A_1$  would be relatively closest in phase. This means that points  $A_0$  and  $A_1$  were most likely to be on the same primary vortex filament. After the location of point  $A_1$  location was identified, hot wire 1 was re-positioned to point  $A_1$ , while hot wire 2 was repositioned to  $(x_3, y_3 (= y_2), z_3)$ . By traversing hot wire 2 along the  $x$  direction at its new position and by recording  $Cr$  at different  $x_3$ , another point (point  $A_2$ ) where the correlation coefficient again reached a maximum could be identified. Since points  $A_0$  and  $A_1$  were supposed to be on the same primary vortex filament and the same could be said about points  $A_1$  and  $A_2$ , the obvious deduction was that all three points were on the same primary vortex filament. By repeating the above process until eventually the entire cylinder span was covered, the time-averaged shape of the entire primary vortex filament could be revealed. It must be noted that in some cases, misleading results could be obtained via the present method. As shown in figure 2(b), if both the shedding angle and spanwise separation  $\Delta z$  were large, with the reference hot wire positioned at  $A_0$ , we may miss point  $A_1$  and instead capture point  $B$ , which is not on the same primary vortex filament as  $A_0$ . Similarly, on the other half of the span, we might capture point  $C$  instead of the correct point  $A_2$ . Points  $B$  and  $C$  were points on the primary vortex filaments that were adjacent to the one where point  $A_0$  resided. This could lead to an erroneous interpretation of the wake flow field. To avoid such a situation,  $\Delta z$  must be kept small. In the present study,  $\Delta z$  was kept at

no more than  $3d$  during the measurements. With a typical longitudinal vortex spacing (distance between two consecutive vortices in the same row) of about  $4d$  at the present  $Re$ , the maximum allowable  $\theta$  is estimated to be about  $\tan^{-1}(2/3)$  or  $33.7^\circ$ . As the vortex-shedding angles  $\theta$  encountered so far are all smaller than  $33.7^\circ$ , the choice of  $\Delta z = 3d$  is considered adequate. Also, since the shedding frequency might vary slightly in the spanwise direction (three-dimensional vortex shedding), a small  $\Delta z$  would also ensure that the shedding frequencies at the two points under consideration were effectively the same, thus improving the accuracy of the measurements. The precision of the results depends mainly on the magnitudes of  $\Delta x$  and  $\Delta z$ . The smaller the magnitudes of  $\Delta x$  and  $\Delta z$ , the more accurate the results will be. However, in practice, a compromise has to be reached between accuracy and time requirement.

Before ending the present section, we must point out that the present method of determining the shape of the primary vortex is based on the assumption that the primary vortex filament is continuous and vortex dislocations are absent. This assumption seems reasonable as the vortex-shedding frequency was found to be either fairly constant or to vary slightly and continuously over the central part of the cylinder span (see Strouhal number results below). It is also reiterated here that the shape of the primary vortex estimated by the present method represents the time-averaged shape.

### 3. Results and discussions

#### 3.1. Parallel vortex shedding induced by control cylinders

As mentioned above, Hammache & Gharib (1989, 1991) first introduced the transverse control cylinder technique (TCCT) in 1989, and the effects of the control cylinders on the main cylinder's wake at low Reynolds numbers had been reported. In the present work, TCCT was applied to show its influence on the main cylinder's wake at a much higher Reynolds number. In order to validate the accuracy of the present experiment and to appreciate fully the effects the control cylinders have on the wake of the main cylinder, experiments were initially conducted without the control cylinders. During the experiments, the velocity of the free stream was maintained constant at  $10.12 \text{ m s}^{-1}$  and the corresponding Reynolds number (based on the free-stream velocity and main cylinder diameter) was  $Re = 1.57 \times 10^4$ . At this Reynolds number, the wake of the circular cylinder falls within the shear-layer transition regime (Williamson, 1996), and owing to end effects the cylinder wake is expected to be three dimensional. Parameters measured in order to reveal the effects of the control cylinders include the vortex-shedding patterns, various aerodynamic parameters such as pressure distribution, drag and lift coefficients and the Strouhal number.

During the initial part of the investigation, the gap between the two control cylinders and the main cylinder ( $L_1$  and  $L_2$ ) were varied but always kept equal to each other ( $L_1 = L_2$ ). By using the method outlined in §2.2.2, the time-averaged shape of the primary vortex was determined for a range of  $L_1 (= L_2)$  from  $1.15D$  to  $1.45D$ , at typical increment of  $\Delta L/D = 0.02$ . After much trial and error, it was found that when  $L_1 = L_2 = 1.26D$ , where  $D$  is the diameter of the control cylinders, the primary vortex was relatively most straight and parallel to the axis of the main cylinder. This magnitude of  $1.26D$  is also referred to as the optimum spacing ( $L_0$ ). The above was taken as the first indication that parallel vortex shedding was induced at this optimum gap size of  $L_1 = L_2 = L_0 = 1.26D$ . Plots of the variation of correlation coefficient between two wake velocity signals with streamwise position  $x_2/d$  for this optimum case of  $L_1 = L_2 = L_0 = 1.26D$  are shown in figure 3, with some details of

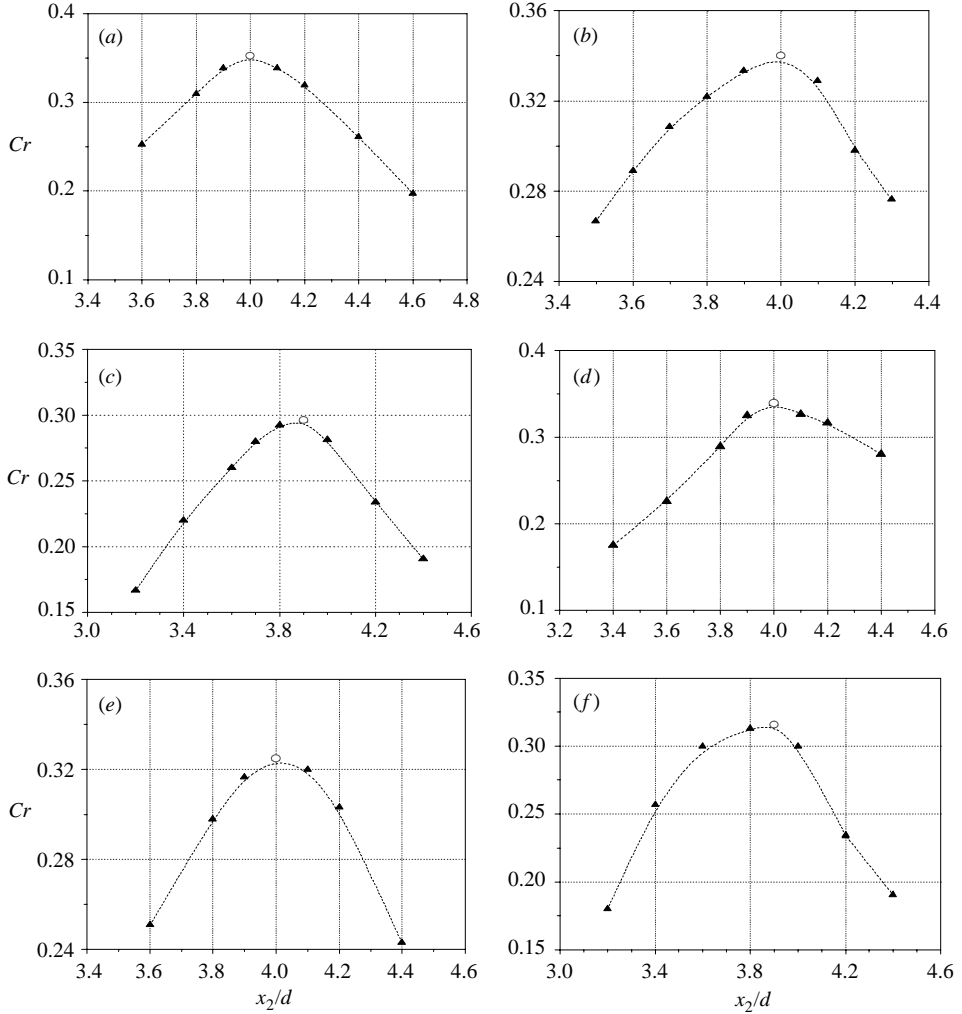


FIGURE 3. Spanwise correlation of the velocity signals to determine the time-averaged vortex-shedding pattern at  $L_1 = L_2 = L_0 = 1.26D$ .  $\circ$ , maximum  $Cr$ . In (a), the reference hot wire (hot wire 1) was placed at  $(4.0d, 0.65d, 0d)$ , while hot wire 2 was placed at  $(x_2, 0.65d, 3d)$  and was traversed along the  $x$ -direction.  $Cr$  versus  $x_2/d$  was noted to reach a maximum at  $x_2 = 4.0d$ . (b) With hot wire 1 displaced to  $(4.0d, 0.65d, 3.0d)$  and hot wire 2 to  $(x_2, 0.65d, 5.5d)$ , the above was repeated and another maximum correlation point was identified at  $(4.0d, 0.65d, 5.5d)$  (c) Hot wire 1  $(4.0d, 0.65d, 5.5d)$ ; hot wire 2  $(x_2, 0.65d, 8.0d)$ ; (d) Hot wire 1  $(4.0d, 0.65d, 0.0d)$ ; hot wire 2  $(x_2, 0.65d, -3.0d)$ ; (e) Hot wire 1  $(4.0d, 0.65d, -3.0d)$ ; hot wire 2  $(x_2, 0.65d, -5.5d)$ ; (f) Hot wire 1  $(4.0d, 0.65d, -5.5d)$ ; hot wire 2  $(x_2, 0.65d, -8.0d)$ .

the process given in the overall caption of figure 3. By noting the  $x_2/d$  magnitude for maximum  $Cr$  at various values of  $z/d$ , the time-averaged shape of the primary Kármán vortex can be deduced. The shape of the primary vortex filament deduced from figure 3, and the one obtained before the inclusion of the control cylinders are plotted and compared in figure 4. It can be seen that before the inclusion of the control cylinders, the (original/natural) vortex filament shed was slightly curved in the convex downstream manner. With the control cylinders optimally placed at  $L_1 = L_2 = 1.26D$ , the vortex filament shed became straight and parallel to the cylinder

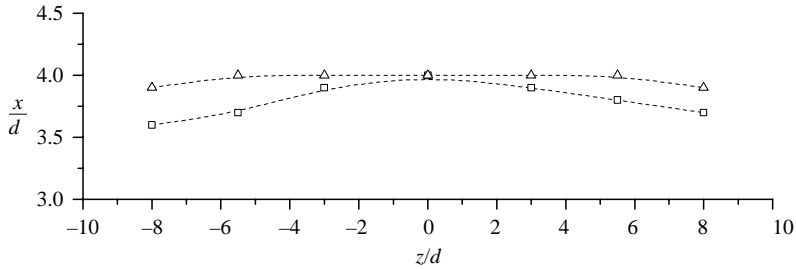


FIGURE 4. Variation in the time-averaged shape of the primary vortex core, with and without control cylinders installed. □, without control cylinders; △, with control cylinders ( $L_1 = L_2 = L_0$ ).

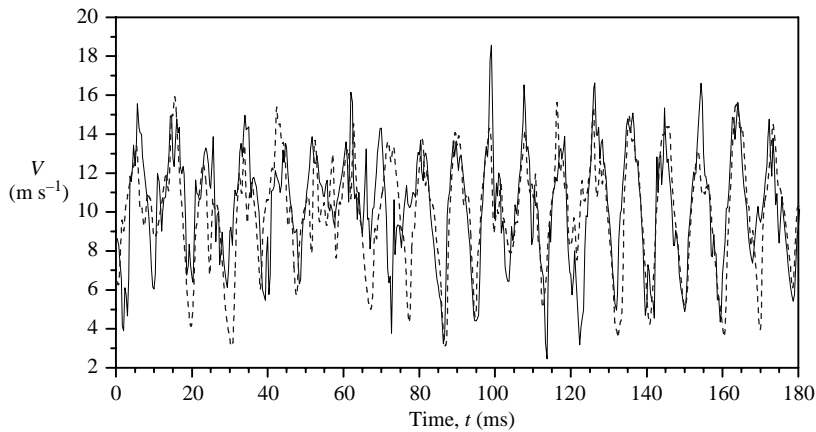


FIGURE 5. Velocity signal traces with —, hot wire 1 at  $(4.0d, 0.65d, 0d)$ , ---, hot wire 2 at  $(4.0d, 0.65d, 3.0d)$  and the control cylinders fixed at the optimum locations. The two velocity signals are practically in phase.

over the spanwise range of  $z/d = -5.5$  to  $z/d = 5.5$ . Beyond the above-mentioned  $z/d$  limits and towards the cylinder ends, the primary vortex curved slightly upstream; this is thought to be due to the influence of the wakes imposed by the control cylinders.

Another way to verify whether parallel vortex shedding has been successfully induced is through studying the traces of wake velocity signals. At the present Reynolds number of  $Re = 1.57 \times 10^4$ , the turbulence level in the cylinder wake was high. The vortex shedding from the main cylinder and the fluctuating wake velocity signal were not highly regular. However, despite this being the case, different wake velocity signals could still be measured and their phase relation studied. Figure 5 shows the two velocity signals recorded simultaneously with a sampling ratio of  $3000 \text{ samples s}^{-1}$ . Hot wire 1 was fixed at point  $(4.0d, 0.65d, 0.0d)$ , and hotwire 2 at point  $(4.0d, 0.65d, 3.0d)$ . During the time interval of 180 ms shown in the plot, it could be seen that the two wake velocity signals, though separated by a spanwise distance of  $\Delta z/d = 3$ , are practically in-phase (during the time period shown in figure 5,  $Cr$  was as high as 0.61). Because the  $x$ -position for both hot wires is the same ( $x_1/d = x_2/d = 4$  in figure 5), the in-phase observation suggests that parallel vortex shedding takes place

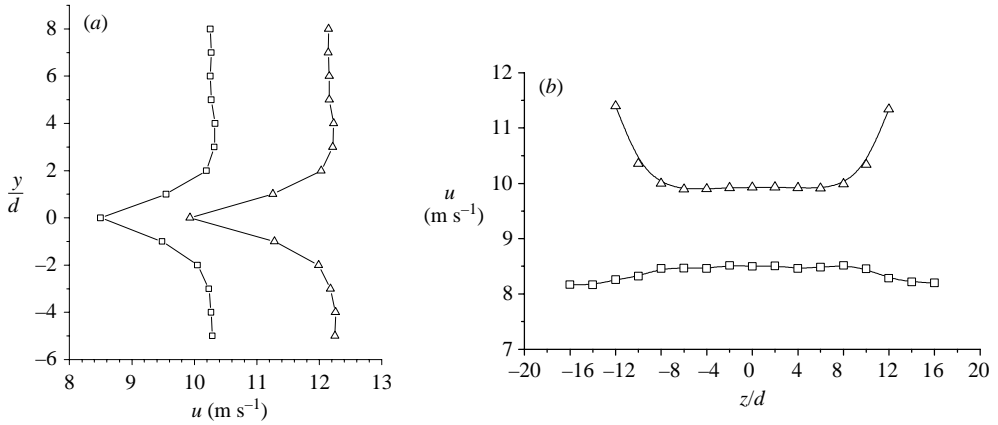


FIGURE 6. Velocity distribution in the cross-flow plane  $x/d = -2.6$ . (a) In  $y$ -direction and at mid-span ( $z/d = 0$ ). (b) In  $z$ -direction and at mid-height ( $y/d = 0$ ). □, before the inclusion of the control cylinders; △, with the control cylinders at the optimum control locations.

at least within the  $z/d$  range of 0 to 3. This finding is consistent with the straight and parallel to cylinder axis primary vortex shape reported in figure 4.

In reference to Williamson (1996), four methods that can minimize the end effects of the wake flow to achieve parallel shedding were mentioned in § 1. All these techniques involve a slight speeding up of the flow near the cylinder ends. With a Pitot-tube, the velocity profile of the approaching flow was measured in the cross-flow plane at  $x/d = -2.6$ , which is a plane  $1.6d$  upstream of the front stagnation line of the main cylinder. Because the front part of the Pitot-tube has to be aligned to the flow when it is used, the crossflow plane of  $x/d = -2.6$  is about the closest (to the main cylinder) upstream plane for which we can carry out velocity distribution measurement. The experimental results are shown in figure 6. Note that both sets of data (with and without control cylinders) were obtained under identical far-field free-stream velocity of  $10.12 \text{ m s}^{-1}$ . Towards the front stagnation point, the velocity of the approaching flow would decelerate gradually to 0. As shown in figure 6(a), before the addition of the control cylinders, the flow velocity decreased to about  $8.4 \text{ m s}^{-1}$  at the sampling location. After the addition of the control cylinders (at  $L_1 = L_2 = L_0$ ), owing to the extra blockage effect (approximately 23.33%), the flow velocity was increased to about  $9.9 \text{ m s}^{-1}$ . Away from the mid-height ( $y/d = 0$ ) region of the test-section (in the regions  $|y/d| > 2$ ), the  $y$ -direction (vertical) velocity distribution was quite uniform. The relatively constant velocity increased from about  $10.3 \text{ m s}^{-1}$  when there were no control cylinders, to about  $12.3 \text{ m s}^{-1}$  after the control cylinders were in position. Figure 6(b) shows that at  $y/d = 0$  and in the cylinder spanwise ( $z$ ) direction and over the region  $-8 \leq z/d \leq 8$ , the flow velocity was increased from  $8.4 \text{ m s}^{-1}$  when there were no control cylinders to around  $9.9 \text{ m s}^{-1}$  when the control cylinders were installed at  $L_1 = L_2 = L_0$ . Results also showed that the control cylinders speeded up the flow near the test-cylinder ends. Before the inclusion of the control cylinder, the velocity near the test-section vertical sidewalls slightly reduces owing to the influence of the wall boundary layers. After the inclusion of the control cylinders, the flow velocity near the cylinder ends was increased, confirming Williamson (1996). For both before and after the inclusion of the control cylinders, the spanwise velocity distributions shown in figure 6(b) suggest that the approaching flow was uniform in the spanwise range of  $-8 \leq z/d \leq 8$ .

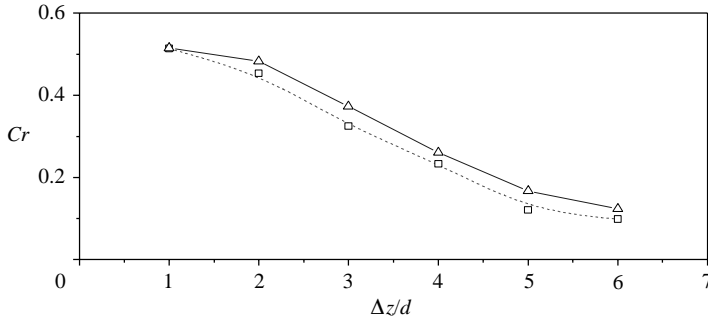


FIGURE 7. Spanwise correlation of the velocity signals with hot wire 1 fixed at  $(4.0d, 0.65d, 0.0d)$  and hot wire 2 in the region  $(4.0d, 0.65d, 1.0d$  to  $6.0d)$ .  $\square$ , no control cylinders;  $\triangle$ , with control cylinders ( $L_1 = L_2 = L_0$ ).

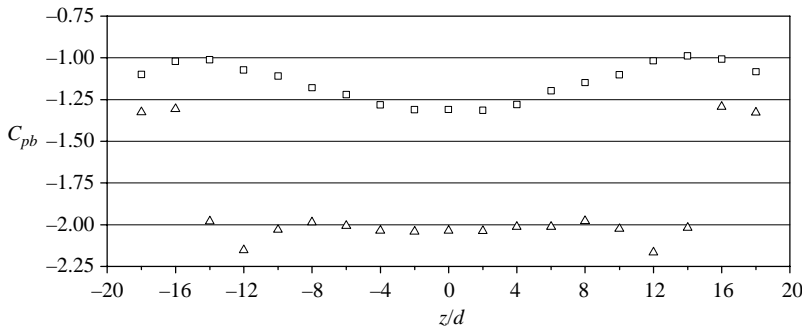


FIGURE 8. Effects of control cylinders on the spanwise time-averaged base pressure ( $C_{pb}$ ) distribution.  $\square$ , before the inclusion of the control cylinders;  $\triangle$ , with the control cylinders at the optimum locations.

### 3.2. Aerodynamic parameters associated with curved and parallel vortex shedding

After parallel vortex shedding has been established, the next issue to address is what are the magnitudes of various aerodynamic parameters that correspond to curved and parallel vortex shedding. In the following various aerodynamic parameters measured from either the main cylinder alone (curved vortex shedding) or with two control cylinders optimally placed (parallel vortex shedding) are compared.

Figure 7 shows the spanwise correlation of the fluctuating velocity ( $Cr$ ) computed over a sampling duration of 10 s. In both cases,  $Cr$  drops with increasing spanwise separation  $\Delta z$ . However, the values of  $Cr$  for parallel shedding are consistently larger than their no control cylinder counterparts. This outcome is anticipated and shows that with the control cylinders placed optimally, the degree of two-dimensionality of the flow had been improved. However, the margin in the increase in  $Cr$  is not very large; we are not sure of the cause of the above observation, but will not rule out the highly irregular flow at the present Reynolds number as a possible factor. It is also noted that the magnitude of  $Cr$  shown in figure 7 is generally low, which is also thought to be a consequence of the irregular nature of the flow.

Pressure measurement showed that the acceleration of the flow near the cylinder ends caused a local pressure reduction. Figure 8 compares the mean (time-averaged) base pressure  $C_{pb}$  ( $C_p$  at  $\beta = 180^\circ$ ) distribution between the two cases. Without the control cylinders, the distribution of  $C_{pb}$  is non-uniform. The lowest (most negative)

pressure takes place at mid-span, and the pressure increases towards the ends of the cylinders, reaching a (least negative) maximum near  $z/d = \pm 14$ . Beyond  $|z/d| = 14$ , the pressure reduces slightly with a further increase in  $|z/d|$ . The spanwise distribution of  $C_{pb}$  therefore suggests that in the absence of the control cylinders, the pressure at the back of the circular cylinder ( $\beta = 180^\circ$ ) is higher near the ends and lower at the mid-span ( $z/d = 0$ ) of the cylinder. This pressure gradient is expected to cause a mid-span-seeking spanwise flow at the back of the cylinder. This mid-span-seeking flow is believed to be responsible for the curved shedding shown in figure 4. In fact, according to Hammache & Gharib (1991), a mid-span-seeking base flow will result in a convex downstream type of curved shedding. This agrees perfectly with the present primary vortex shape shown in figure 4. The inclusion of the control cylinders caused a pressure reduction near  $z/d = \pm 12$ , as shown in figure 8. With the control cylinders installed at the most optimum positions ( $L_1 = L_2 = L_0$ ), which speeds the flow up in the region  $|z/d| > 8$  (figure 6*b*), the base pressure becomes more negative over effectively the entire span. However, the spanwise pressure gradient is now greatly reduced and the base pressure is now more uniform over the region  $-10 < z/d < 10$ . Beyond that, (i.e.  $|z/d| > 10$ ),  $C_{pb}$  first decreases, but later increases towards the ends of the cylinder. The last bit of increasing trend is believed to be under the influence of the wakes of the control cylinders, axes of which were located at  $z/d = \pm 16$ . It is believed that since the base pressure over  $-10 < z/d < 10$  has become more uniform, the vortex shedding over that central part of the cylinder span has also become more parallel. Figure 9 presents the mean surface pressure variation over the rear half of the cylinder ( $|\beta| \geq 90^\circ$ ), before and after the inclusion of the control cylinders. They clearly demonstrate the more uniform spanwise pressure distribution over the rear half of the test cylinder when the control cylinders were at the optimum control locations. This is taken as the second indication that parallel vortex shedding has been achieved.

In the present work, a large number of main cylinder time-averaged surface-pressure data were acquired, both with and without control cylinders. It is impossible to present all of them here. To illustrate the differences between curved and parallel vortex shedding, selected circumferential pressure distributions of the main cylinder are shown in figure 10. In figure 10(*a*), the mid-span ( $z/d = 0$ ) pressure ( $C_p$ ) distribution (without blockage correction) of the main cylinder (without control cylinders) are compared to the data of West & Apelt (1981, 1982) at similar Reynolds number. It can be seen that the agreement among the data is good, and this endorses the accuracy of the present data. In figure 10(*b*), the mid-span ( $z/d = 0$ ) pressure ( $C_p$ ) distribution (without blockage correction) of the main cylinder for the case of no control cylinders was compared to the case of control cylinders optimally placed. It can be seen that the presence of the optimally placed control cylinders reduces the surface pressure on the main cylinder throughout its entire circumference, except the front stagnation point, but there is no noticeable shift in the flow-separation positions. This suggests that the presence of the optimally placed control cylinders is likely to result in an increase in the time-averaged drag force on the main cylinder. This will be further discussed below. Figure 10(*c*) is similar to figure 10(*b*), except that it is for the circumferential pressure ( $C_p$ ) distribution at  $z/d = 8$ . The difference in the two pressure distributions is similar to figure 10(*b*), thus again suggesting that the higher time-averaged drag is associated with the case of control cylinders optimally placed. However, careful examination further reveals that while the set of pressure data that corresponds to the case of control cylinders optimally placed is quite close to the corresponding set of data in figure 10(*b*), the set of data that corresponds to the case

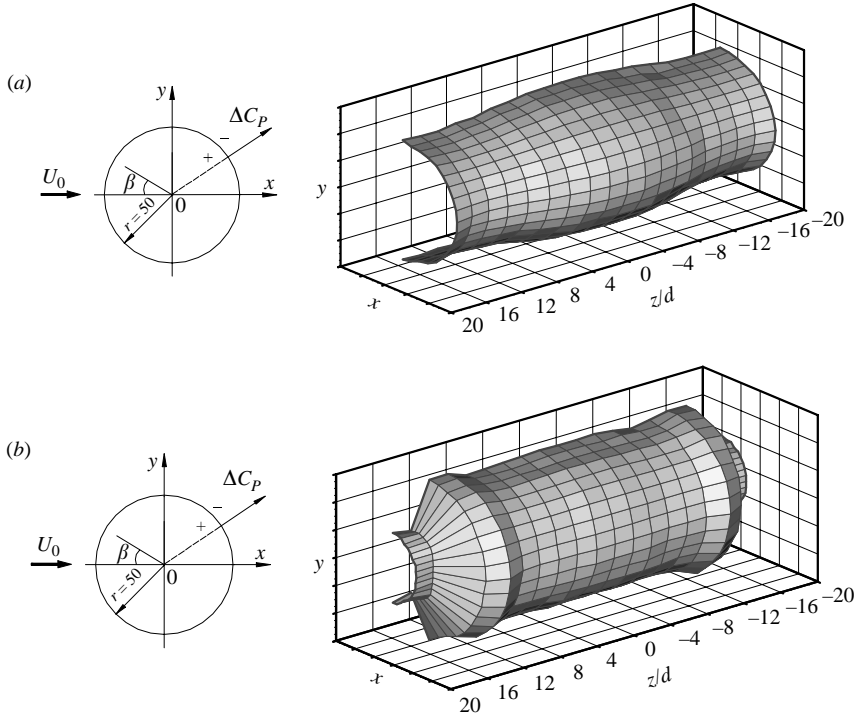


FIGURE 9. Time-averaged surface-pressure variation over the rear half ( $|\beta| \geq 90^\circ$ ) of the cylinder. (a) Without control cylinders. (b) With control cylinders at the optimum locations of  $L_1 = L_2 = L_0$ . To make the pressure variation more apparent, the pressure difference is calculated from  $\Delta C_{P,i} = (C_{P,i} - \bar{C}_P) \times 50$ , where  $C_{P,i}$  is the mean pressure coefficient at each measurement point,  $\bar{C}_P = (1/n) \sum_{i=1}^n C_{P,i}$  is the mean value of the pressure coefficient over the rear half of the cylinder, and 50 is a convenient magnification factor.

of no control cylinders in figure 10(c) indicates that the pressure in the wake region is slightly higher (less negative) than its counterpart in figure 10(b). This suggests that the base pressure is slightly higher near the ends of the main cylinder than at mid-span, a finding which we already know from the  $C_{pb}$  data shown in figure 8. The implication of this point will be further discussed below.

Based on the time-averaged pressure distribution, the time-averaged drag coefficient ( $C_D$ ) and lift coefficient ( $C_L$ ) were calculated and plotted in figure 11 for both the cases of no control cylinders and with the control cylinders at  $L_1 = L_2 = L_0$ . For  $C_L$ , in both cases, the magnitude remains effectively zero over the whole span which is expected from symmetry consideration. For  $C_D$ , without control cylinders it is at a maximum magnitude of about 1.238 at mid-span. This magnitude of 1.238 is in quite good agreement with the magnitude of  $C_D$  reported by a number of workers in the literature at similar Reynolds number, one of which is West & Apelt (1982). (Note: from figure 5 of West & Apelt (1982), at Reynolds number very similar to the present work, we estimated their  $C_D$  to be 1.235 and 1.24 for cases with blockage ratio of 3.5% and 5.5%, respectively.) After blockage correction by using the method reported in Maskell (1963), our mid-span drag coefficient is reduced to  $C_{Dc} = 1.2$ . In the present paper, an extra subscript 'c' is used to indicate that the quantity concerned is blockage-effects compensated. From the mid-span,  $C_D$  decreases gradually towards the cylinder ends. For the case of parallel shedding (control cylinders installed at

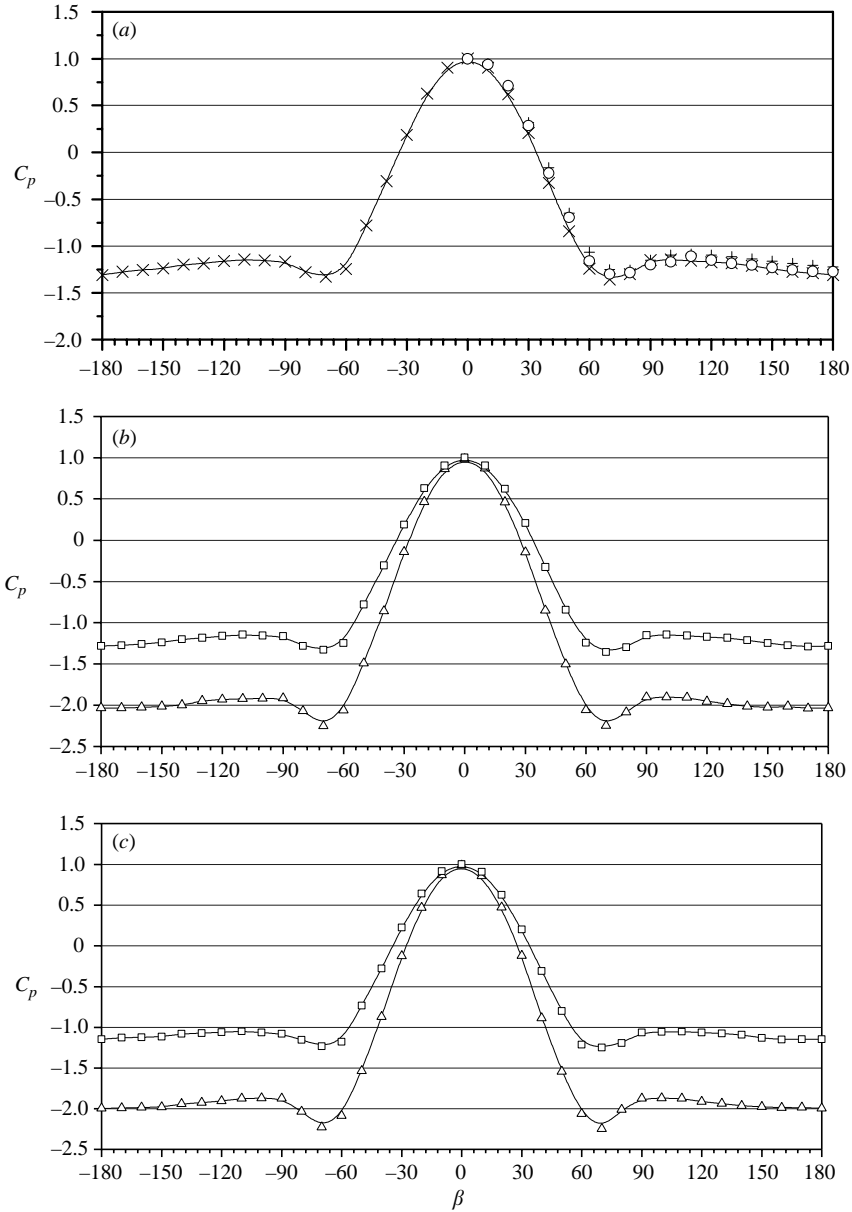


FIGURE 10. Circumferential distribution of mean  $C_p$ . (a)  $C_p$  at  $z/d=0$ ,  $\times$ , present data;  $+$ , West & Apelt (1981),  $Re=1.5 \times 10^4$ , blockage ratio = 5.8%;  $\circ$ , West & Apelt (1982),  $Re=3 \times 10^4$ , blockage ratio = 5.8%,  $H/d=6$ . (b)  $C_p$  at  $z/d=0$ ,  $\square$ , main cylinder only;  $\triangle$ , with control cylinders optimally placed. (c)  $C_p$  at  $z/d=8$ , same symbols as (b).

$L_1=L_2=L_0$ ), within the range of  $z/d=-10$  to  $10$ , the values of  $C_D$  were fairly constant but at a higher magnitude of about 1.6. This larger  $C_D$  appears to be due mainly to the increase in the rear face suction on the main cylinder when the control cylinders were optimally placed. In the regions  $|z/d| > 12$ ,  $C_D$  drops rapidly to minima of approximately 0.2 at  $z/d=\pm 16$ , the locations of the control cylinders. The drop in local  $C_D$  there is because that part of the main cylinder is directly within the wakes

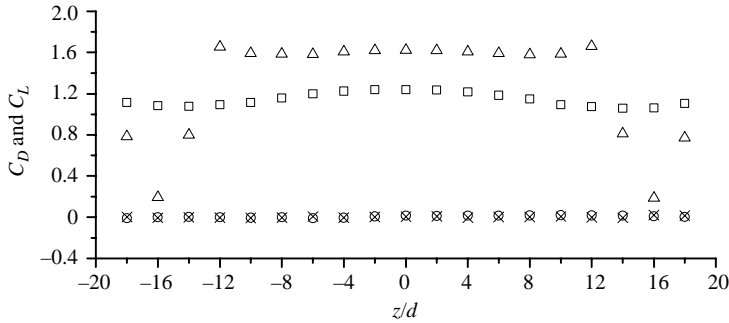


FIGURE 11. Spanwise distribution of time averaged  $C_L$  and  $C_D$ , with and without control cylinders.  $\square$ ,  $C_D$  without control cylinders;  $\triangle$ ,  $C_D$  with the control cylinders at the optimum locations  $L_1 = L_2 = L_0$ ;  $\times$ ,  $C_L$  without control cylinders;  $\circ$ ,  $C_L$  with control cylinders at the optimum locations  $L_1 = L_2 = L_0$ .

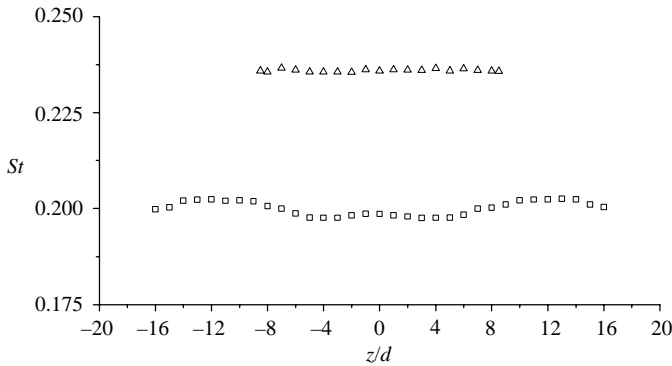


FIGURE 12. Spanwise distribution of  $St$ .  $\square$ , before addition of the control cylinders;  $\triangle$ , with the control cylinders at the optimum control distance.

of the control cylinders. To end the discussion on drag coefficient, we must point out that the much larger drag coefficient of 1.6 is at least partially a consequence of the large blockage introduced by the control cylinders. The present configuration of one main cylinder with two larger transverse control cylinders located near its ends is such that no known accurate blockage-correction method is available for application. The magnitude of a blockage-influence-free two-dimensional flow (parallel vortex shedding) drag coefficient at the present Reynolds number is likely to be less than 1.6, but its exact magnitude is not known at present. In § 4 of this paper, we will present an attempt to estimate approximately the effects of blockage when the control cylinders are present. However, this (blockage effects when control cylinders are present) issue requires further careful investigation. Some preliminary work by the first author and another student had already begun.

The spanwise distribution of the Strouhal number is plotted in figure 12. Without the control cylinders, the magnitude of the  $St$  is around 0.199 near the mid-span of the main cylinder. This is again in good agreement with the typical  $St$  magnitude quoted in the literature, which includes the work by West & Apelt (1982). (Note: from figure 10 of West & Apelt (1982), at about the same Reynolds number as the present work, we estimated their Strouhal number to be 0.198 for the case with a blockage ratio of 5.8 %.) After blockage correction, our mid-span Strouhal

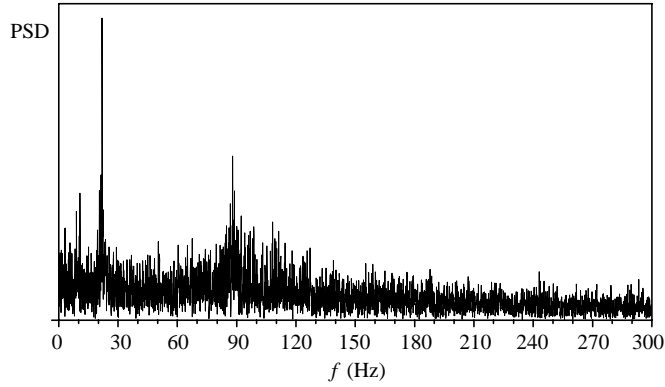


FIGURE 13. Power spectrum of the main cylinder wake velocity signal near the cylinder end with the hot wire fixed at  $(4.0d, 0.65d, -9.0d)$ , Control cylinders were at optimum locations (i.e.  $L_1 = L_2 = L_0 = 1.26D$ ).

number becomes  $St_c = 0.195$ . With changing  $z/d$ ,  $St$  slightly decreases to about 0.198 at  $z/d = \pm 5$  before it gradually increases to around 0.20 near  $z/d = \pm 12$ . Thereafter,  $St$  slightly drops towards the cylinder ends. For parallel shedding,  $St$  remains quite uniform over the central span ( $-8 < z/d < 8$ ) and the magnitude increases to about 0.236. The uniform spanwise distribution of  $St$  is taken as a third indication that the vortex shedding over that part of the span is parallel. Beyond the spanwise region of  $z/d = -8.0$  to  $z/d = 8.0$ , two shedding frequencies were detected in the wake of the main cylinder. The power spectrum of the velocity at  $z/d = -9.0$  is shown in figure 13. A peak was observed near  $f_{s,1} = 89$  Hz, and another at about  $f_{s,2} = 23$  Hz. This was so because the wake flow near the ends of the main cylinder was also under the influence of the control cylinders. The peak at  $f_{s,1}$  ( $= 89$  Hz) is due to the shedding of vortices from the main cylinder, while the peak at  $f_{s,2}$  ( $= 23$  Hz) is caused by vortices shed by the control cylinders. Note that the diameter of the control cylinders ( $= 100$  mm) is four times that of the test cylinder ( $= 25$  mm). Since it is known from literature that the Strouhal number is fairly constant in the sub-critical Reynolds-number range, it is therefore anticipated that the control cylinders should shed vortices at about a quarter the frequency of the test cylinder ( $23 \text{ Hz} / 89 \text{ Hz} = 0.258$ ).

As reported earlier, with the main cylinder alone,  $St_c$  near the mid-span is 0.195. For circular cylinder vortex shedding, Fey, König & Eckelmann (1998) proposed a new Strouhal–Reynolds-number relation of

$$St = St^* + \frac{m}{\sqrt{Re}}. \quad (5)$$

Coefficients  $St^*$  and  $m$  vary for different ranges of Reynolds number. In the present study,  $Re = 1.57 \times 10^4$  and the aspect ratio  $L/d = 40$ . In this range,  $St^* = 0.1776$  and  $m = 2.2023$  (for detailed information of coefficients  $St^*$  and  $m$ , see Fey *et al.* 1998). The Strouhal number estimated by their formula is

$$St = 0.1776 + \frac{2.2023}{\sqrt{1.57 \times 10^4}} = 0.1952.$$

This value agrees well with the present experiment's mid-span Strouhal number of  $St_c = 0.195$ .

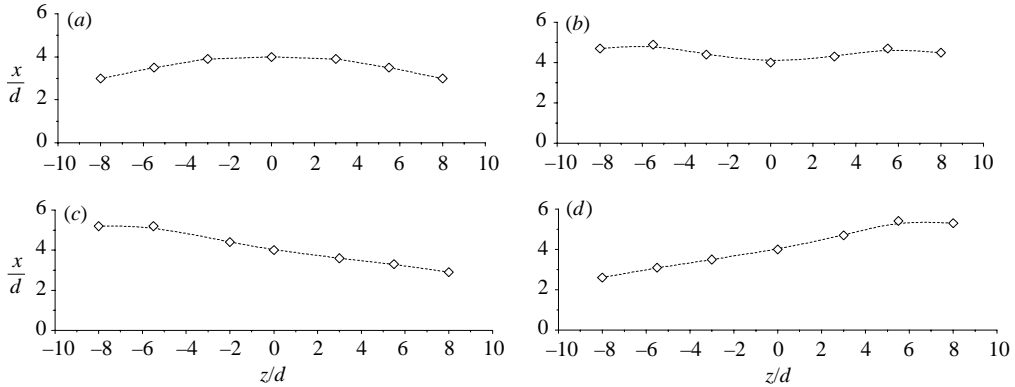


FIGURE 14. Various time-averaged primary vortex shapes with the control cylinders located at difference distances  $L$  to the main cylinder. (a)  $L_1 = L_2 = 1.5D$ ; (b)  $L_1 = L_2 = 1.0D$ ; (c)  $L_1 = 1.0D, L_2 = 1.5D$ ; (d)  $L_1 = 1.75D, L_2 = 0.75D$ .

### 3.3. Effects of the control cylinder distance $L$

#### 3.3.1. Time-averaged shape of the primary vortex

Experimental results showed that the control distance  $L$  affects the vortex-shedding geometries in ways similar to the situation reported at low Reynolds number. Both curved and oblique vortex shedding were observed when the control cylinders were at different control distances. As shown in figure 14(a), when the control cylinders were placed at a distance larger than the optimum distance  $L_0$ , i.e.  $(L_1 = L_2) > L_0$ , with  $L_1 = L_2 = 1.5D$ , the shape of the primary vortex is curved in a convex downstream manner over the range of  $z/d = -8.0$  to  $8.0$ , and is symmetrical about mid-span. When the gaps between the control cylinders and the main cylinder are reduced to  $(L_1 = L_2) < L_0$ , the shape of the primary vortex becomes concave downstream and symmetrical with respect to mid-span. It was also observed that the vortex-shedding pattern became oblique when the control cylinders were positioned such that  $L_1 \neq L_2$ . Figure 14(c) shows the case for  $L_1 < L_0 < L_2$ , with  $L_1 = 1.0D$  and  $L_2 = 1.5D$ . Over the span from  $z/d = -5.5$  to  $5.5$ , the shedding filament was linear and oblique. Figure 14(d) presents the results of  $L_1 > L_0 > L_2$ , with  $L_1 = 1.75D$  and  $L_2 = 0.75D$ , the vortex-shedding pattern remained oblique, but the sign of the oblique angle became opposite to that when  $L_1 < L_0 < L_2$ . All these observations agree well with Hammache & Gharib's (1989, 1991) investigation in the laminar vortex shedding regime. One difference here is that for  $|z/d| > 5.5$ , the primary vortex changes direction and turns slightly upstream, which is thought to be due to the influence of the control cylinder wakes. It also seems that the oblique shedding angle increases with the difference between  $L_1$  and  $L_2$ . For the case of  $L_1 < L_0 < L_2$ ,  $\Delta L = L_1 - L_2 = -0.5D$ , the shedding angle was  $\theta = -9.8^\circ$ . For the case of  $L_1 > L_0 > L_2$ ,  $\Delta L = L_1 - L_2 = 1.0D$ , the shedding angle becomes  $\theta = 11.81^\circ$  ( $\theta$  is calculated from  $\theta = \tan^{-1}(\Delta x / \Delta z)$ ).

#### 3.3.2. Spanwise time-averaged base pressure distribution

For other cases of oblique and curved vortex shedding, the effects of the control cylinders on the base pressure distribution of the main cylinder were investigated. The results are plotted in figure 15. When the control cylinders are at equi-distance from the main cylinder (i.e.  $L_1 = L_2$ ), the reduction in base pressure at both ends (with the control cylinders installed, by 'ends' here we are referring approximately to  $z/d = \pm 8$ ) of the main cylinder are the same, this usually results in a primary vortex

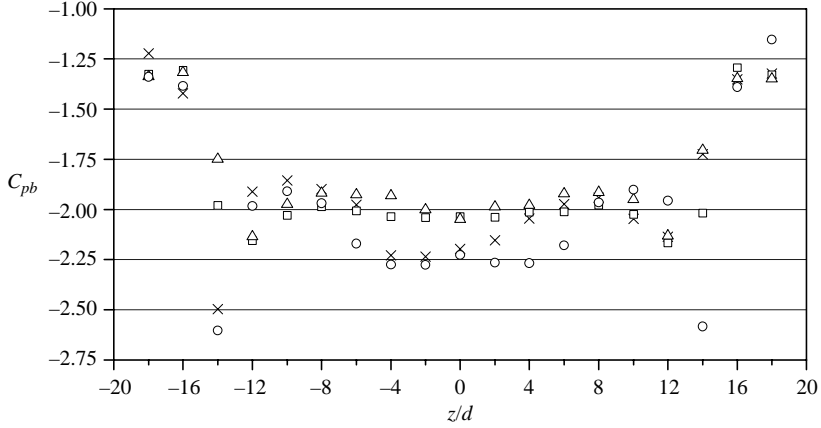


FIGURE 15.  $C_{pb}$  ( $C_p$  at  $\beta = 180^\circ$ ) versus  $z/d$  with control cylinders at various distances from the main cylinder.  $\times$ ,  $L_1/D = 1.0$ ,  $L_2/D = 1.5$ ;  $\square$ ,  $L_1/D = L_2/D = 1.26$ ;  $\triangle$ ,  $L_1/D = L_2/D = 1.5$ ;  $\circ$ ,  $L_1/D = L_2/D = 1.0$ .

with a shape that is symmetrical with respect to mid-span. When  $L_1 (= L_2)$  varies, the reduction (to become more negative) in cylinder end static pressure also varies and in such a way that a large  $L$  will result in a small cylinder end static pressure reduction and vice versa. At a certain optimum distance ( $L_0$ ), the reduction in cylinder end static pressure nearly completely neutralizes the original spanwise pressure gradient. Under this circumstance, the wake spanwise pressure gradient over the central part of the span ( $-8 \leq z/d \leq 8$  in the present case) nearly disappears (i.e. becomes very small), and the vortex shedding becomes parallel (two-dimensional shedding) over the central part of the cylinder span. As reported earlier, in the present study, the optimum distance  $L_0$  is  $1.26D$ . With the control cylinders at  $L_1 = L_2 > L_0$ , the influences of the control cylinders are insufficient (under-correction), in the wake the cylinder end pressures are still higher than mid-span pressure (see figure 15 for the case  $L_1 = L_2 = 1.5D > L_0$ ), this results in a spanwise base flow from the cylinder ends to mid-span, and eventually leads to a convex downstream vortex-shedding pattern (figure 14a) that is similar to no control cylinders, as shown in figure 8. With the control cylinders located closer to the test cylinder at  $L_1 = L_2 < L_0$ , the control cylinder influences become too strong (over-correction), in the wake, the pressure was slightly higher at mid-span than points on both sides of it (here we are referring to the approximate region of  $-4 \leq z/d \leq 4$ ), the spanwise flow was from mid-span towards the cylinder ends, and this results in a concave downstream type of shedding pattern, as shown in figure 14(b).

When  $L_1 \neq L_2$ , the imposed static pressure at the two ends of the cylinder become unequal, this causes a spanwise pressure gradient and results in oblique vortex shedding. As shown in figure 14(c), with the control cylinder asymmetrically positioned at  $L_1 (= 1.0D) < L_0$ , and  $L_2 (= 1.5D) > L_0$ , the vortex shedding becomes oblique. From figure 15, the  $C_{pb}$  distribution gradually increases from  $z/d = -4$  to 8, this causes spanwise flow from  $z/d = 8$  to  $-4$ , and induces oblique shedding, with a shedding angle of  $\theta = -9.8^\circ$ . With the control cylinders at  $L_1 (= 1.75D) > L_0$  and  $L_2 (= 0.75D) < L_0$ , the shedding angle becomes positive with  $\theta = 11.8^\circ$ . As mentioned earlier, it also appears that the magnitude of the oblique shedding angle increases with increasing difference between  $L_1$  and  $L_2$ . Relative to the cylinder, the obliquely

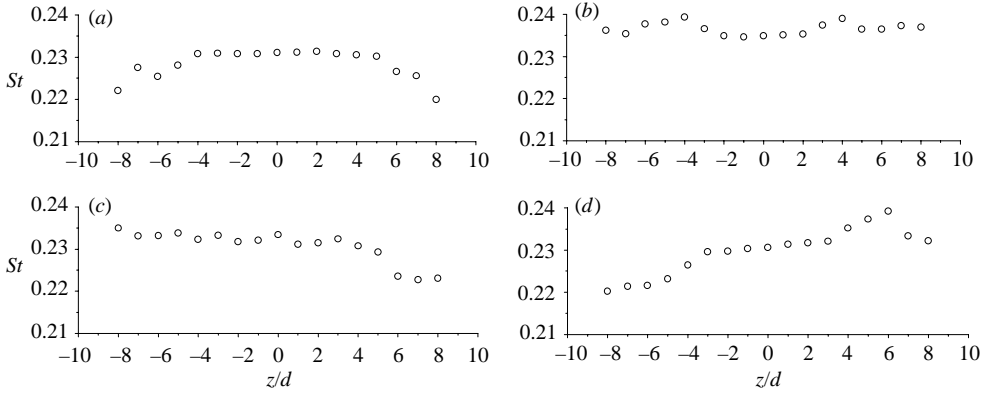


FIGURE 16. Spanwise distribution of  $St$  with the control cylinders located at different distances  $L$  to the test cylinder. (a)  $L_1 = L_2 = 1.5D$ ; (b)  $L_1 = L_2 = 1.0D$ ; (c)  $L_1 = 1.0D$ ,  $L_2 = 1.5D$ ; (d)  $L_1 = 1.75D$ ,  $L_2 = 0.75D$ .

shed vortex is always slanted in the same way as the straight line joining the centres of the control cylinders.

#### 3.4. Relationship between the Strouhal number for oblique and parallel vortex shedding – The cosine law

The Strouhal number spanwise distributions that correspond to the four cases illustrated in figure 14 are shown in figure 16. As can be seen, in all the cases with the presence of the control cylinders,  $St$  remains generally constant over the spanwise extent of approximately  $-4.0 \leq z/d \leq 4.0$  and  $-3.0 \leq z/d \leq 3.0$  for sub-figures (a), (c) and sub-figures (b), (d), respectively. Beyond the above-mentioned  $z/d$  range,  $St$  shows large variation, and can either increase or decrease towards the cylinder ends. The variation is dependent on the position of the control cylinders and is thought to be due to the influence of the control cylinder wake.

In an attempt to find a relation between the parallel vortex-shedding and oblique vortex-shedding Strouhal number, we subjected our Strouhal number data to the cosine law proposed by Williamson (1988). As shown in figure 12, for the case of parallel vortex shedding, the Strouhal number ( $St_0$ ) remains quite constant over the central part of the span of  $-8 \leq z/d \leq 8$ , and the mean value is  $St_0 = 0.2360$ . For the oblique vortex shedding shown in figure 14(c), the shedding angle is  $\theta = -9.8^\circ$ . According to the cosine law, the Strouhal number for the oblique shedding ( $St_\theta$ ) would be

$$\begin{aligned} St_\theta &= St_0 \cos \theta \\ &= 0.2360 \times \cos(-9.8^\circ) = 0.2326. \end{aligned} \quad (6)$$

As for the oblique vortex shedding shown in figure 14(d), the shedding angle is  $\theta = 11.81^\circ$ . By using (6) again, we obtain  $St_\theta = 0.2310$ . For these two oblique vortex-shedding cases, the mean value of  $St$  computed from the data shown in figures 16(c) and 16(d) and within the  $z/d$  range of  $z/d = -4$  to  $4$  is  $0.2321$  and  $0.2308$ , respectively. In both cases, the values of  $St_\theta$  estimated by the cosine law are in very close agreement to the experimentally measured  $St_\theta$ , demonstrating the validity of the cosine law in the present flow at  $Re$  of  $O(10^4)$ .

#### 4. Overall discussion and conclusions

From the vast amount of information reported in the literature, it is known that primary (von Kármán) vortices shed by a circular cylinder only remain straight and parallel to the cylinder up to a fairly low Reynolds number of about 72 (Hammache & Gharib 1989). From  $Re=72$  to some value just below 200 (different values had been reported by different workers, but this upper limit is typically quoted to be somewhere between 158 to 194), vortices shed are slanted with respect to the cylinder. From results shown in papers such as Hammache & Gharib (1991), it appears that the cause of a non-parallel vortex shedding is the non-uniform (spanwise direction) base pressure of the circular cylinder. Four different methods, which all resulted in slightly speeding up the flow near the ends of the cylinder, resulting in an uniform spanwise base pressure distribution, had been reported (Williamson 1996) to be able to induce parallel vortex shedding in the  $Re$  range of 72 to 158–194. As pointed out in Prasad & Williamson (1997), there is little work that attempts to apply those methods that work at low Reynolds number to induce parallel vortex shedding at moderate to high Reynolds number. In fact, to the best of our knowledge, only Prasad & Williamson (1997) reported that parallel vortex shedding had been induced at  $Re=200$  to 10000. Prasad & Williamson induced parallel vortex shedding by inclining the cylinder end plates (with diameter 16 times that of the cylinder) in a toe-in manner by  $12^\circ$ . Prasad & Williamson's results are essentially smoke-wire-flow visualization and hot-wire measurements. In the present paper, with the intention of contributing towards the 'void of parallel vortex shedding at moderate to high Reynolds number', our objective is to find out whether one of the four methods that are known to induce parallel vortex shedding at low Reynolds number, namely the transverse control cylinders technique (TCCT) initially pioneered by Hammache & Gharib (1989, 1991), will work at a much higher Reynolds number of  $1.57 \times 10^4$ , based on Hammache & Gharib (1989)'s suggestion that for the TCCT to work effectively, the ratio of the control to main cylinder diameter ( $D/d$ ) must be greater than 3. With minimizing blockage effects in mind, we designed our experiment around a  $D/d$  value of 4. After much trial and error, we found that by positioning the control cylinders at distances of  $L_1 = L_2 = 1.26D$  upstream of the main cylinder, the latter was induced to shed time-averaged parallel vortices at  $Re = 1.57 \times 10^4$ . The supporting evidence we obtained included the primary vortices shed being found to be straight and parallel to the main cylinder axis, the time-averaged surface pressure over the rear half of the cylinder becoming uniform in the spanwise direction over a certain central part of the cylinder span, and the Strouhal number being constant over a certain central part of the cylinder span.

Next, we measured aerodynamic parameters of the main cylinder under two circumstances, at identical far-field Reynolds numbers  $1.57 \times 10^4$  ( $U_\infty = 10.12 \text{ m s}^{-1}$ ). (i) When the main cylinder was by itself (the natural case), shedding curve primary vortices in the convex downstream manner. (ii) When control cylinders were placed at  $L_1 = L_2 = L_0 = 1.26D$ , and the main cylinder (the induced case) shed (time-averaged) straight and parallel (to cylinder axis) primary vortices. In the first case, at the cylinder mid-span, we measured the following parameter magnitudes, all time-averaged quantities after wind-tunnel-blockage correction by the method of Maskell (1963):  $C_{Lc} \approx 0$ ,  $C_{Dc} = 1.2$ ,  $C_{pbc} = -1.22$ ,  $St_c = 0.195$ . The magnitudes of these parameters were found to be in very good agreement with those reported in the literature, such as West & Apelt (1981, 1982). The magnitude of our measured Strouhal number was also found to be in good agreement with the prediction by Fey *et al.* (1998)'s  $St-Re$

relation. In the second case, we measured  $C_L \approx 0$ ,  $C_D = 1.6$ ,  $C_{pb} = -2.03$ ,  $St = 0.236$  (all time-averaged quantities).

At other control cylinder gap sizes, we found that with equal gap size at the two ends of the main cylinder, the (time-averaged) primary vortex shed was curved, and was either concave or convex in the downstream direction, depending on whether the gaps were smaller or larger than the optimum size of  $L_0$  of  $1.26D$ , respectively. When the sizes of the two gaps were different, (time-averaged) oblique primary vortices were shed. The primary vortices were found to be inclined to the main cylinder in the same way as the straight line joining the centres of the two control cylinders. The oblique angle was also found to vary with the difference in the gap size between the two ends of the main cylinder. At the present (fairly high) Reynolds number of  $1.54 \times 10^4$ , the relation between the oblique and parallel vortex-shedding Strouhal number ( $St_\theta$  and  $St_0$ , respectively) was found still to follow the cosine law proposed by Williamson (1988).

Spanwise base pressure distribution data measured in the present work support the explanation given in Hammache & Gharib (1991) that a non-uniform spanwise base pressure will induce a spanwise flow in the base region of the cylinder, resulting in either curved or oblique vortex shedding, details of which depend on the exact form of spanwise base pressure variation. When this spanwise base pressure variation is eliminated, primary vortices shed will become straight and parallel to the cylinder axis. From the data collected, it seems that when a spanwise base flow is eliminated (two-dimensional case), the base pressure will become lower (more negative) than when a spanwise base flow exists (three-dimensional case), resulting in larger drag coefficient, while the associated vortex-shedding frequency (Strouhal number) had increased. However, as pointed out earlier in the paper, the magnitude of the aerodynamic parameters associated with parallel vortex shedding are under the influence of appreciable wind-tunnel blockage ( $\approx 23.33\%$ ). Such a large blockage is an inherent part of the TCCT, and is likely to affect the aerodynamic parameters. At present, no known correction method is available to compensate for the blockage effects of such cylinder geometry. However, based on the principle of invariance under constraint (Engineering Science Data Unit (ESDU) 80024 1980), blockage effects can be equated to an uniform increase in reference velocity. (Note: as mentioned in ESDU80024, the assumption of invariance is strictly an approximation, but past work had demonstrated that it works reasonably well for blockage area ratio of up to 10–15%). With this principle, the following formula can be derived.

$$\frac{C_{Dc}}{C_D} = \left( \frac{U_\infty}{U_\infty + \Delta U_\infty} \right)^2 = \frac{1 - C_{pc}}{1 - C_p} = \left( \frac{St_c}{St} \right)^2. \quad (7)$$

In (7), the subscript 'c' (as elsewhere in this paper) refers to quantities that are compensated for blockage effects, and  $\Delta U_\infty$  is the blockage effect equivalent change in reference velocity. In the present work, the magnitude of  $\Delta U_\infty$  is not known. However, as an approximation just for the sake of illustrating the magnitude of the blockage effect influence, in reference to figure 6(a), we estimate  $\Delta U_\infty$  to be  $2 \text{ m s}^{-1}$ . Our estimation is based on the fact that in figure 6(a), away from  $y/d = 0$ , the flow velocity at  $x/d = -2.6$  is approximately  $10.3 \text{ m s}^{-1}$  and  $12.3 \text{ m s}^{-1}$  for the cases of without and with control cylinders installed, respectively; and we therefore estimate  $\Delta U_\infty$  to be equal to the difference between the two above-mentioned velocities ( $= 2 \text{ m s}^{-1}$ ). With  $U_\infty = 10.12 \text{ m s}^{-1}$  and  $\Delta U_\infty = 2 \text{ m s}^{-1}$ , and with  $C_D = 1.6$ ,  $C_{pb} = -2.03$  and  $St = 0.236$  (for the case of control cylinders at optimum locations), we get  $C_{Dc} = 1.1155$ ,

$C_{pbc} = -1.1125$  and  $St_c = 0.1971$ . These figures are surprisingly close to the magnitudes of  $C_{Dc} = 1.2$ ,  $C_{pbc} = -1.22$  and  $St_c = 0.195$  for the blockage effect compensated main cylinder. While we reiterate that  $\Delta U_\infty = 2 \text{ m s}^{-1}$  is only an approximate (guessed) value, in the absence of more accurate values to apply, the above calculation nevertheless demonstrates that a significant part of the change in aerodynamic parameters is likely to be caused by the extra blockage incurred when the control cylinders were installed. (Note: the above approximate estimation of the effects of blockage was initially suggested by one of the reviewers of this paper. The contribution of this anonymous reviewer is hereby gratefully acknowledged.) It would be interesting to find what magnitude the above-mentioned aerodynamic parameters assume when the blockage effects are either absent or eliminated. This is one of the aspects that we intend to further investigate in the future.

As many real life engineering structures resemble circular cylinders, the magnitude and frequency of forces acting on them are important numbers. We believe that by understanding the cause(s) of the various types of vortex shedding and the magnitude of the associated aerodynamic parameters, we would be able eventually to reduce the magnitude of undesirable forces and avoid (or reduce the risk of) flow-induced vibration of structures.

#### REFERENCES

- BERGER, E. 1964 Transition of the laminar vortex flow to the turbulent state of the Karman vortex street behind an oscillating cylinder at low Reynolds number. *Jahrb. Wiss. Gess. LR*, 164.
- BERGER, E. & WILLE, R. 1972 Periodic flow phenomena. *Annu. Rev. Fluid Mech.* **4**, 313–340.
- EISENLOHR, H. & ECKELMANN, H. 1989 Vortex splitting and its consequence in the vortex street wake of cylinders at low Reynolds numbers. *Phys. Fluids. A* **1**, 189–192.
- ENGINEERING SCIENCE DATA UNIT 80024 1980 Blockage corrections for bluff bodies in confined flows.
- FEY, U., KÖNIG, M. & ECKELMANN, H. 1998 A new Strouhal–Reynolds-number relationship for the circular cylinder in the range  $47 < Re < 2 \times 10^5$ . *Phys. Fluids.* **10**, 1547–1549.
- GASTER, M. 1971 Vortex shedding from circular cylinders at low Reynolds numbers. *J. Fluid Mech.* **46**, 749–756.
- HAMMACHE, M. & GHARIB, M. 1989 A novel method to promote parallel vortex shedding in the wake of circular cylinders. *Phys. Fluids. A* **1**, 1611–1614.
- HAMMACHE, M. & GHARIB, M. 1991 An experimental study of the parallel and oblique shedding from circular cylinders. *J. Fluid Mech.* **232**, 567–590.
- MASKELL, E. C. 1963 A theory of blockage effects on bluff bodies and stalled wings in a closed wind tunnel. *ARC R & M*, no. 3400.
- MAULL, D. J. & YOUNG, R. A. 1973 Vortex shedding from bluff bodies in a shear flow. *J. Fluid Mech.* **60**, 401–409.
- MILLER, G. D. & WILLIAMSON, C. H. K. 1994 Control of three-dimensional phase dynamics in a cylinder wake. *Exps. Fluids.* **18**, 26–35.
- PRASAD, A. & WILLIAMSON, C. H. K. 1997 Three-dimensional effects in turbulent bluff body wakes. *Exp. Thermal Fluid Sci.* **14**, 9–16.
- RAMBERG, S. E. 1983 The effects of yaw and finite length upon the vortex wakes of stationary and vibrating circular cylinders. *J. Fluid Mech.* **128**, 81–107.
- SIAOUTI, A. & GERRARD, J. H. 1981 An experimental investigation of the end effects on the wake of a circular cylinder towed through water at low Reynolds numbers. *J. Fluid Mech.* **112**, 297–314.
- TRITTON, D. J. 1959 Experimental on the flow past a circular cylinder at low Reynolds numbers. *J. Fluid Mech.* **6**, 547–567.
- VAN ATTA, C. W. & GHARIB, M. 1987 Ordered and chaotic vortex streets behind circular cylinders at low Reynolds numbers. *J. Fluid Mech.* **174**, 113–133.

- WEST, G. S. & APELT, C. J. 1981 Blockage and aspect ratio effects on flow past a circular cylinder for  $10^4 < Re < 10^5$ . *University of Queensland, Civil Engng Res. Rep.* CE23.
- WEST, G. S. & APELT, C. J. 1982 The effects of tunnel blockage and aspect ratio on the mean flow past a circular cylinder with Reynolds numbers between  $10^4$  and  $10^5$ . *J. Fluid Mech.* **114**, 361–377.
- WILLIAMSON, C. H. K. 1988 Defining a universal and continuous Strouhal–Reynolds number relationship for the laminar vortex shedding of a circular cylinder. *Phys. Fluids* **31**, 2742–2744.
- WILLIAMSON, C. H. K. 1989 Oblique and parallel modes of vortex shedding in the wake of a circular cylinder at low Reynolds numbers. *J. Fluid Mech.* **206**, 579–628.
- WILLIAMSON, C. H. K. 1996 Vortex dynamics in the cylinder wake. *Annu. Rev. Fluid Mech.* **28**, 477–539.